ELSEVIER

Journal of Magnetism and Magnetic Materials 248 (2002) 164–180

journal of magnetism and magnetic materials

www.elsevier.com/locate/jmmm

General spin wave instability theory for anisotropic ferromagnetic insulators at high microwave power levels

A.V. Nazarov*, C.E. Patton, R.G. Cox, L. Chen, P. Kabos

Department of Physics, Colorado State University, Fort Collins, CO 80523, USA

Received 18 December 2001

Abstract

The theory of spin wave instability for ferromagnetic insulators is extended to include generalized anisotropy based on a tensor formulation of the static and dynamic effective fields. The formalism is set up for saturated magnetic ellipsoids and a general microwave field configuration. Both first- and second-order processes are considered. The analysis yields working formulae for the threshold microwave field amplitude evaluations and critical mode determinations. An example is given for first-order processs in a thin disk with easy plane anisotropy.

PACS: 76.50

Keywords: Spin waves; Ferrites; Non-linear magnetics; Magnetic anisotropy; Microwave technology

1. Introduction

Spin wave instability is a non-linear process which occurs in ferrite magnetic materials when the applied microwave magnetic field reaches a critical value. At this critical field, energy is transferred from the microwave field to parametrically excited spin wave pairs with the same frequency and equal and opposite wave vectors. Spin wave instability processes can be categorized in various ways. Following Suhl [1], the terms "first order" and "second order" may be used to denote processes in which the parametric spin waves are at one-half the pump frequency or at the pump frequency, respectively. The initial theory developed by Suhl [1], Schlömann [2], and Schlömann et al. [3] considered resonance saturation (RA), a second-order process, and subsidiary absorption (SA) and parallel pumping (PP) first-order processes. These formulations were for isotropic ferrites. Only circularly polarized transverse pumping and linearly polarized parallel pumping microwave field configurations were considered.

In order to deal with real ferrite materials and microwave fields which approximate device environments, it is necessary to extend the above theories to include anisotropy and more general pumping configurations. Oblique pumping with a general polarization for the microwave field was considered by Yakovlev [4], Green et al. [5], and Patton [6,7]. These treatments considered only

*Corresponding author. Tel.: +1-970-491-4056; fax: +1-970-491-7947.

E-mail address: alexn@lamar.colostate.edu (A.V. Nazarov).

0304-8853/02/$ - see front matter
PII: S0304-8853(02)00171-3

first-order processes. The Suhl–Schlömann first-order analysis was also extended to include cubic anisotropy by Haubenreisser et al. [8,9], Petrakovskii [10], Yakovlev [11], and Patton [12]. Refs. [8,10] were for parallel pumping, Ref. [9] was for transverse pumping, Refs. [11,12] were for a general oblique pumping configuration. The high power response of unaxial and planar ferrites has been studied by numerous authors [13–21]. These papers consider first- and second-order effects, RS, SA, and PP processes, and non-collinear magnetization field configurations.

Most of the above theories were concerned with special cases. None provide a fully general theoretical framework for the analysis of first- and second-order processes in a material of general shape, with a general anisotropy, or for a possibly non-collinear magnetization and field. The purpose of this work was to develop such a theory. The formalism is for a magnetic insulator of ellipsoidal-shaped with a general free energy-based magnetic anisotropy and a general microwave field configuration.

This new formulation is based on the formalism of Ref. [1] and the general effective field approach given in Ref. [12]. The theory considers only spin waves in the short wavelength limit for which sample surface effects can be neglected. The analysis yields working formulae for the threshold microwave field amplitude for spin wave instability, specified as h_c, as a function of the spin wave decay rate and the spin wave wave vector $\mathbf{k}$. The spin wave decay rate is expressed in linewidth units through a "spin wave linewidth" parameter ΔH_k. The h_c threshold is $\mathbf{k}$ dependent. For a specific material, sample shape, static magnetic field, and microwave frequency and pumping configuration, one may determine the minimum h_c and the corresponding critical mode $\mathbf{k}$ for this minimum. This minimum threshold, denoted below as h_{crit}, should correspond to the microwave threshold observed experimentally. A summary of the theory was recently published in Ref. [21].

The formalism can be used in two ways. First, if ΔH_k is known or can be estimated for a given material and pumping configuration, the theory can be used to obtain the h_{crit} threshold and the corresponding critical mode. Conversely, one can measure h_{crit} vs. static field and use the theory to fit the data to obtain values of ΔH_k. In some cases, this second procedure can also allow one to determine ΔH_k as a function of $\mathbf{k}$. Both applications are crucial for the full analysis of high power microwave thresholds in ferrite materials and a complete understanding of the relevant spin wave instability processes.

Section 2 establishes the laboratory frame sample and field geometry for the problem. Section 2 also establishes the fundamental dynamic response and effective field equations needed for the analysis. This is done for an ellipsoidal shape sample and a general anisotropy based on free energy considerations. Section 3 introduces the concept of a precession reference frame for the analysis of the dynamic response and establishes operating equations for static equilibrium. Section 4 incorporates the formalism established above to develop coupled equations for the spin wave amplitudes and working equations for spin wave instability. Section 5 develops working equations for the uniform precession mode. Section 6 combines the results of the previous sections to obtain operational expressions for the threshold microwave field amplitude for spin wave instability under the general conditions outlined above. Finally, Section 7 gives an example calculation for first processes in a typical Y-type hexagonal ferrite with planar anisotropy. Curves of the threshold microwave field h_{crit} vs. the static external field H_{ext} as well as results on the associated critical modes are presented. Gaussian cgs units are employed throughout.

2. Sample geometry and effective fields

Fig. 1 shows the basic sample geometry for the problem. One has an ellipsoidal-shaped single domain ferrite sample with principal axes along, X, Y, and Z. The externally applied uniform static magnetic field $\mathbf{H}_{ext}$ has polar and azimuthal angles θ_H and φ_H in the (X, Y, Z) *laboratory frame*. The static magnetization vector $\mathbf{M}_s$ has polar and azimuthal angles θ_M and φ_M, respectively. In general, $\mathbf{H}_{ext}$ and $\mathbf{M}_s$ will not be collinear. The static equilibrium orientation of $\mathbf{M}_s$ will be

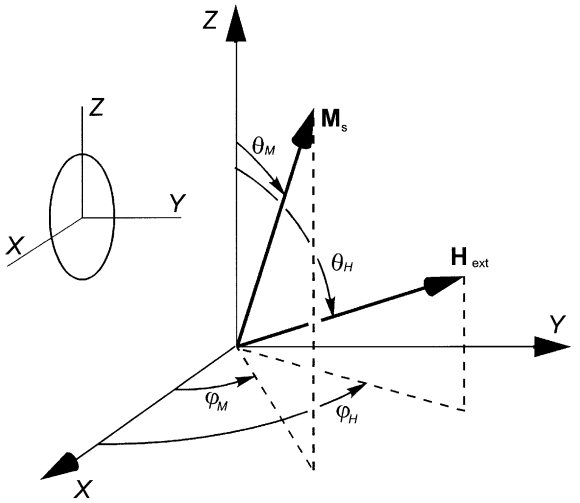

Fig. 1. The laboratory (X, Y, Z) frame. The external static field $\mathbf{H}_{ext}$ is applied at a polar angle θ_H and an azimuthal angle φ_H. The static magnetization $\mathbf{M}_s$ lies at a polar θ_M and an azimuthal angle φ_M. The inset shows that the coordinate axes (X, Y, Z) coincide with the principal directions of the ellipsoidal sample.

determined by direction of $\mathbf{H}_{ext}$, the sample shape and corresponding demagnetizing factors N_X, N_Y, and N_Z, and the anisotropy of the material. These considerations will be developed shortly.

In order to solve the combined static and dynamic problems, it is necessary to develop analytic expression for the static and dynamic problems effective fields. One may start this process with a magnetization vector written in the form

$$\mathbf{M} = \mathbf{M}_s + \mathbf{m}. \tag{1}$$

In general, the dynamic magnetization $\mathbf{m}$ is a function of time t and position $\mathbf{r}$ in the sample, and may be expanded as a spatial Fourier series according to

$$\mathbf{m}(\mathbf{r}, t) = \sum_{\mathbf{k}} \mathbf{m}_{\mathbf{k}}(t) e^{i\mathbf{k}\cdot\mathbf{r}}, \tag{2}$$

where $\mathbf{k}$ denotes the wave vector for a given spin wave. The term for $\mathbf{k} = 0$ corresponds to the uniform mode response $\mathbf{m}_0$. From here on, references to $\mathbf{m}(\mathbf{r}, t)$ will be given simply as $\mathbf{m}$.

One may also write the total effective magnetic field as $\mathbf{H}_{eff}$ and break this field down into various physical terms according to [12]

$$\mathbf{H}_{eff} = \mathbf{H}_{ext} + \mathbf{H}_D + \mathbf{H}_A + \mathbf{h}_{ex} + \mathbf{h}, \tag{3}$$

where $\mathbf{H}_D$ denotes the Maxwellian field due to sample shape demagnetizing effects and magnetic dipole interactions within the sample, $\mathbf{H}_A$ is an effective field due to anisotropy, $\mathbf{h}_{ex}$ is an effective field due to exchange, and $\mathbf{h}$ denotes the applied external microwave field. The $\mathbf{H}_D$ and $\mathbf{H}_A$ fields contain both static and dynamic components. The exchange field is a dynamic field. The convention to use lower case letters to denote dynamic fields will be followed here.

The $\mathbf{H}_D$ term in Eq. (3) consists of a static term and two dynamic terms. The static term represents a demagnetizing field of the form $-4\pi\mathbf{N}'\mathbf{M}_s$, where $\mathbf{N}'$ is the diagonal demagnetizing tensor in the (X, Y, Z) laboratory frame of Fig. 1. For the ellipsoid sample inset of Fig. 1, the diagonal elements $\mathbf{N}'$ may be taken as $N'_{XX} = N_X, N'_{YY} = N_Y, N'_{ZZ} = N_Z$. N_X, N_Y, and N_Z denote the usual ellipsoidal sample demagnetizing factors. These demagnetizing factors will turn out to be important parameters in the theory. The first dynamic term is the dynamic demagnetizing field counterpart to the above static field, $-4\pi\mathbf{N}'\mathbf{m}_0$. The second dynamic term in $\mathbf{H}_D$ is the dipole field associated with the spin waves. In the short wave length limit, this field may be written as

$$\mathbf{h}_{dip} = -4\pi \sum_{k\neq 0} \frac{\mathbf{k}(\mathbf{k}\cdot\mathbf{m}_k)}{k^2} e^{i\mathbf{k}\cdot\mathbf{r}}. \tag{4}$$

Turn now to the effective non-Maxwellian anisotropy field. The components of $\mathbf{H}_A$ may be written as

$$H_{A,i} = -\frac{1}{M_s}\frac{\partial}{\partial\alpha_i} F_A = -\frac{\partial}{\partial M_i} F_A, \quad i = (X, Y, Z), \tag{5}$$

where $F_A(\alpha_x, \alpha_y, \alpha_z)$ defines a general anisotropy free energy [22], and α_x, α_y, and α_z are the direction cosines of $\mathbf{M}$ relative to X-, Y-, and Z-axis in Fig. 1, respectively. It is important to realize that the $\mathbf{M}$ vector itself consists of a static component $\mathbf{M}_s$, as in Fig. 1, and the additional dynamic component introduced above. If the condition $|\mathbf{m}| \ll |\mathbf{M}_s|$ is satisfied, the static and dynamic terms in $\mathbf{M}$, when folded into Eq. (5), lead to $\mathbf{H}_A$

components of the form

$$H_{\mathrm{A},i} = H_{\mathrm{A},i}(\mathbf{M}_\mathrm{s}) + \sum_{j=1}^{3} \left.\frac{\partial H_{\mathrm{A},i}(\mathbf{M})}{\partial M_j}\right|_{\mathbf{M}=\mathbf{M}_\mathrm{s}} m_j. \tag{6}$$

The first term on the right-hand side of Eq. (6) corresponds to a *static* effective anisotropy field which depends only on $\mathbf{M}_\mathrm{s}$. This vector field will be denoted as $\mathbf{H}_{\mathrm{AS}}$. The second term represents the dynamic part of $\mathbf{H}_\mathrm{A}$. This vector field will be denoted as $\mathbf{h}_\mathrm{A}$. The field $\mathbf{h}_\mathrm{A}$ has the form $\mathbf{A}'\mathbf{m}$, where $\mathbf{A}'$ is an anisotropy tensor with components given by

$$A'_{ij} = -\left.\frac{\partial^2 F_\mathrm{A}(\mathbf{M})}{\partial M_i \partial M_j}\right|_{\mathbf{M}=\mathbf{M}_\mathrm{s}}. \tag{7}$$

It is clear that $\mathbf{A}'$ is a symmetric tensor.

The only remaining field terms in Eq. (3) are the effective exchange field and the applied microwave field. The exchange field may be written as $|\gamma| D\nabla^2\mathbf{m}/M_\mathrm{s}$, where $|\gamma|$ is the absolute value of the electron gyromagnetic ratio and D is the exchange stiffness field parameter [22]. Detailed nomenclature for the applied microwave field $\mathbf{h}$ will be introduced later.

From the effective fields established above, one may now separate the static and dynamic contributions to $\mathbf{H}_\mathrm{eff}$. The static terms combine to yield a static effective field given by

$$\mathbf{H}^\mathrm{s}_\mathrm{eff} = \mathbf{H}_\mathrm{ext} - 4\pi\mathbf{N}'\mathbf{M}_\mathrm{s} + \mathbf{H}_\mathrm{AS}. \tag{8}$$

This vector field will be a function of the various parameters established above and, in particular, the direction of $\mathbf{M}_\mathrm{s}$. The magnetization $\mathbf{M}_\mathrm{s}$ will be in static equilibrium when the condition

$$\mathbf{M}_\mathrm{s} \times \mathbf{H}^\mathrm{S}_\mathrm{eff} = 0 \tag{9}$$

is satisfied, such that $\mathbf{M}_\mathrm{s}$ and $\mathbf{H}^\mathrm{S}_\mathrm{eff}$ are collinear. The complete dynamic part of $\mathbf{H}_\mathrm{eff}$ may now be written as

$$\mathbf{h}_\mathrm{eff} = -4\pi \sum_{k\neq 0} \frac{\mathbf{k}(\mathbf{k}\cdot\mathbf{m}_\mathrm{k})}{k^2} \mathrm{e}^{\mathrm{i}\mathbf{k}\cdot\mathbf{r}} - 4\pi\mathbf{N}'\mathbf{m}_0 + \mathbf{A}'\mathbf{m} + \frac{1}{M_\mathrm{S}}|\gamma| D\nabla^2\mathbf{m} + \mathbf{h}. \tag{10}$$

The next section will consider the dynamics of the magnetization in a new (x, y, z) coordinate system for which the z-axis coincides with the direction of $\mathbf{M}_\mathrm{s}$ under conditions of static equilibrium. In this new reference frame, termed the *precession frame*, the uniform mode part of the dynamic $\mathbf{m}$ response will correspond to a Larmor precession of $\mathbf{M}$ about the z-axis. The static effective field in this frame will have only a z-component. The total dynamic field in Eq. (10) will be transformed into this frame. This will result in a precession frame equation of motion for the dynamic magnetization, or torque equation, which leads to the non-linear coupled equations which are needed for the analysis of spin wave instability.

3. Transformation to the precession frame

Consider the rotational transformation shown in Fig. 2 from the (X, Y, Z) laboratory frame to the (x, y, z) precession frame. The angles θ_M and φ_M are the same angles as introduced in Fig. 1 for static equilibrium. The transformation of any general vector $\mathbf{R}$ in the laboratory frame to the corresponding vector $\mathbf{r}$ in the (x, y, z) frame may be written in the form $\mathbf{r} = \mathbf{TR}$, where the $\mathbf{T}$ matrix is

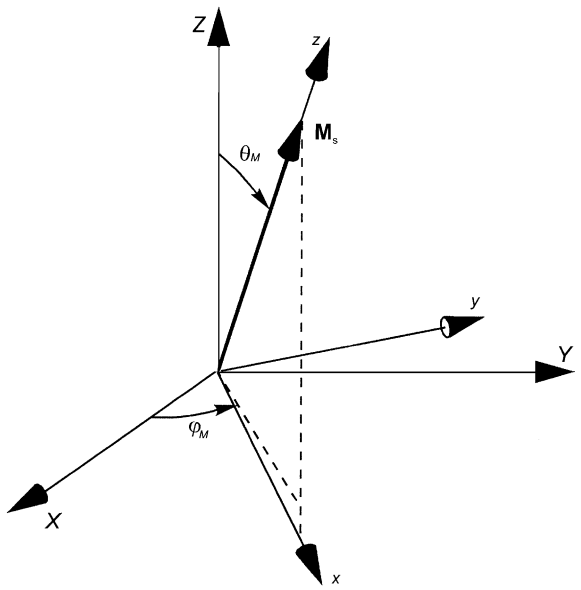

Fig. 2. Transformation from the (X, Y, Z) laboratory frame to the (x, y, z) precession frame. The z-axis coincides with the direction of the static magnetization $\mathbf{M}_\mathrm{s}$. The static magnetization $\mathbf{M}_\mathrm{s}$ lies at a polar angle θ_M and an azimuthal angle φ_M.

given by

$$\mathbf{T} = \begin{pmatrix} \cos\theta_{\mathrm{M}}\cos\varphi_{\mathrm{M}} & \cos\theta_{\mathrm{M}}\sin\varphi_{\mathrm{M}} & -\sin\theta_{\mathrm{M}} \\ -\sin\varphi_{\mathrm{M}} & \cos\varphi_{\mathrm{M}} & 0 \\ \sin\theta_{\mathrm{M}}\cos\varphi_{\mathrm{M}} & \sin\theta_{\mathrm{M}}\sin\varphi_{\mathrm{M}} & \cos\theta_{\mathrm{M}} \end{pmatrix}. \quad (11)$$

The transformation of the various vector fields and tensors enumerated above to the (x, y, z) frame is straightforward. The elements of the demagnetizing tensor in the (x, y, z) frame, $\mathbf{N} = \mathbf{T}\mathbf{N}'\mathbf{T}^{-1}$, are given by

$$N_{xx} = (N_X \cos^2\varphi_M + N_Y \sin^2\varphi_M)\cos^2\theta_M + N_Z \sin^2\theta_M, \quad (12)$$

$$N_{yy} = N_X \sin^2\varphi_M + N_Y \cos^2\varphi_M, \quad (13)$$

$$N_{zz} = (N_X \cos^2\varphi_M + N_Y \sin^2\varphi_M)\sin^2\theta_M + N_Z \cos^2\theta_M, \quad (14)$$

$$N_{xy} = N_{yx} = (N_Y - N_X)\cos\theta_M \sin(2\varphi_M)/2, \quad (15)$$

$$N_{xz} = N_{zx} = (N_X \cos^2\varphi_M + N_Y \sin^2\varphi_M - N_Z) \times \sin(2\theta_M)/2, \quad (16)$$

and

$$N_{yz} = N_{zy} = (N_Y - N_X)\sin\theta_M \sin(2\varphi_M)/2. \quad (17)$$

The static demagnetizing field in the (x, y, z) frame is $-4\pi\mathbf{N}(M_s\hat{\mathbf{z}})$, where $\hat{\mathbf{z}}$ is a unit vector in the z-direction. The dynamic demagnetizing field is given by $-4\pi\mathbf{N}\mathbf{m}_0$, where $\mathbf{m}_0$ is given in terms of (x, y, z) frame components.

In the same way, one can obtain the effective anisotropy fields in the (x, y, z) frame. The specific form of $\mathbf{H}_{\mathrm{AS}}$ will depend on the form of the anisotropy energy F_{A} and the angles θ_M and φ_M. The dynamic anisotropy field in the precession frame will be taken as

$$\mathbf{h}_{\mathrm{A}} = \mathbf{A}\mathbf{m} = \mathbf{T}\mathbf{A}'\mathbf{T}^{-1}\mathbf{m} = \begin{pmatrix} A_{xx} & A_{xy} & A_{xz} \\ A_{xy} & A_{yy} & A_{yz} \\ A_{xz} & A_{yz} & A_{zz} \end{pmatrix} \begin{pmatrix} \mathbf{m}_x \\ \mathbf{m}_y \\ \mathbf{m}_z \end{pmatrix}. \quad (18)$$

Since $\mathbf{A}'$ is a symmetric tensor and $\mathbf{T}$ corresponds to a unitary transformation, the matrix $\mathbf{A}$ is also symmetric. The specific form of the elements of $\mathbf{A}$ will also depend on the form of the anisotropy energy F_{A} and the static equilibrium magnetization angles θ_M and φ_M which define the precession frame.

The exchange and dipole fields depend only on the dynamic magnetization $\mathbf{m}$. The form of these fields is the same for the laboratory and the precession frames and the appropriate terms in Eq. (10) apply. The microwave field $\mathbf{h}$ may also be specified directly in the precession frame.

Turn now to static equilibrium considerations. In the precession frame, the zero torque condition of Eq. (9) requires that the x and y components of $\mathbf{H}_{\mathrm{eff}}^{\mathrm{S}}$ vanish. This condition leads to two equations which determine the static equilibrium values of θ_M and φ_M,

$$H_{\mathrm{ext}}[\sin\theta_H\cos\theta_M\cos(\varphi_H - \varphi_M) - \cos\theta_H\sin\theta_M] = 2\pi M_s(N_X\cos^2\varphi_M + N_Y\sin^2\varphi_M - N_Z) \times \sin 2\theta_M + H_{\mathrm{AS},Z}\sin\theta_M - (H_{\mathrm{AS},X}\cos\varphi_M + H_{\mathrm{AS},Y}\sin\varphi_M)\cos\theta_M \quad (19)$$

and

$$H_{\mathrm{ext}}\sin\theta_H\sin(\varphi_M - \varphi_H) = H_{\mathrm{AS},X}\cos\varphi_M - H_{\mathrm{AS},Y}\sin\varphi_M + 2\pi M_s(N_X - N_Y)\sin 2\varphi_M \sin 2\theta_M. \quad (20)$$

The $H_{\mathrm{AS},X}$, $H_{\mathrm{AS},Y}$, and $H_{\mathrm{AS},Z}$ terms in Eqs. (19) and (20) refer to the components of $\mathbf{H}_{\mathrm{AS}}$ in the laboratory frame. Note that Eqs. (19) and (20) are for a general anisotropy. The above equilibrium conditions define the precession frame. In this frame, the static effective field $\mathbf{H}_{\mathrm{eff}}^{\mathrm{S}}$ reduces to one component along z which is given by

$$H_{\mathrm{eff}}^{\mathrm{S}} = H_{\mathrm{ext}}\sin\theta_H\sin\theta_M\cos(\varphi_H - \varphi_M) + H_{\mathrm{ext}}\cos\theta_H\cos\theta_M - 4\pi M_s[N_Z\cos^2\theta_M + (N_X\cos^2\varphi_M + N_Y\sin^2\varphi_M)\sin^2\theta_M] + (H_{\mathrm{AS},X}\cos\varphi_M + H_{\mathrm{AS},Y}\sin\varphi_M)\sin\theta_M + H_{\mathrm{AS},Z}\cos\theta_M. \quad (21)$$

One now has expressions for all static and dynamic fields in the precession frame. The static effective field $\mathbf{H}_{\mathrm{eff}}^{\mathrm{S}}$ is parallel to $\mathbf{M}_s$ and along z. The dynamic effective field $\mathbf{h}_{\mathrm{eff}}$, in general, has non-vanishing components along all three directions in the precession frame. Except for the external microwave field $\mathbf{h}$, all the terms in $\mathbf{h}_{\mathrm{eff}}$ derive from $\mathbf{m}$ through Eq. (10) but expressed in

the (x, y, z) frame. Following Suhl [1], it will prove convenient to write the transverse components of the dynamic magnetization and field in scalar complex form according to

$$m_{\pm} = m_x \pm \mathrm{i} m_y \tag{22}$$

and

$$h_{\mathrm{eff}\pm} = h_{\mathrm{eff},x} \pm \mathrm{i} h_{\mathrm{eff},y}, \tag{23}$$

where $h_{\mathrm{eff},x}$ and $h_{\mathrm{eff},y}$ denote the x and y components of $\mathbf{h}_{\mathrm{eff}}$, respectively. The constant magnetization condition $|\mathbf{M}| = M_{\mathrm{s}}$ then leads to a dynamic magnetization z component of the form

$$m_z = -(m_x^2 + m_y^2)/2 = -m_+ m_-/2. \tag{24}$$

Eq. (24) is valid in the limit $|\mathbf{m}| \ll |\mathbf{M}_{\mathrm{s}}|$ introduced above.

4. Spin wave instability

In the Suhl approach, spin wave instability results from the analysis of the non-linear terms in the torque equation of motion. The details of this procedure will be evident from the development below. One starts with the torque equation of motion for the general magnetization vector $\mathbf{M}$ [23]

$$\frac{\mathrm{d}\mathbf{M}}{\mathrm{d}t} = -|\gamma| \mathbf{M} \times \mathbf{H}_{\mathrm{eff}}. \tag{25}$$

Based on the precession frame formulation of the dynamic magnetization and effective fields as given above, one can use Eq. (25) to obtain the equations of motion for the spin wave amplitudes. This is accomplished through a plane wave Fourier expansion for the dynamic components of $\mathbf{M}$ in the precession frame. One then considers specific pairs of terms in this expansion for $\pm\mathbf{k}$, where $\mathbf{k}$ is a general spin wave wave vector. Terms with $\mathbf{k} = 0$ correspond to the uniform mode. Such terms, when present, are connected with components of the microwave field which are transverse to the z-direction.

As the first step, one obtains expressions for $\dot{m}_+$ and $\dot{m}_-$ from Eq. (25). These may be written as

$$-\mathrm{i}\dot{m}_+ = |\gamma| m_+ (H_{\mathrm{eff}}^{\mathrm{S}} + h_{\mathrm{eff},z}) - |\gamma| (M_{\mathrm{s}} + m_z) h_{\mathrm{eff}+} \tag{26}$$

and the corresponding equation for $\dot{m}_-$, where $h_{\mathrm{eff},z}$ denotes the z component of $\mathbf{h}_{\mathrm{eff}}$. The $m_{\pm}$ variables are now expanded in Fourier series in the form

$$m_+ = M_{\mathrm{s}} \sum_{\mathbf{k}} a_{\mathbf{k}} \mathrm{e}^{\mathrm{i}\mathbf{k}\cdot\mathbf{r}} \tag{27}$$

and

$$m_- = M_{\mathrm{s}} \sum_{\mathbf{k}} a_{-\mathbf{k}}^* \mathrm{e}^{\mathrm{i}\mathbf{k}\cdot\mathbf{r}}. \tag{28}$$

The sums in Eqs. (27) and (28) specifically include the uniform mode at $\mathbf{k} = 0$ and $\mathbf{k} \neq 0$ terms which span the full range of allowed values for bulk spin waves. As indicated in the introduction, the non-zero $\mathbf{k}$ terms are taken to be in the short wave length limit for which surface effects can be neglected. For convenience, the vector nomenclature for $\mathbf{k}$ will be dropped from subscripts from here on. Note that a_0 corresponds to a normalized complex uniform mode amplitude, while the a_k factors with $\mathbf{k} \neq 0$ correspond to classical spin wave amplitudes [23]. Unless otherwise noted, references to a_k will always imply the $\mathbf{k} \neq 0$ condition and a_0 will specifically denote the uniform mode.

Direct substitution of the various field terms developed above into Eq. (26) and the corresponding $\dot{m}$ equation, along with the expressions for m_+, m_-, and m_z, yields a set of non-linear coupled equations for the a_k and a_{-k}^* spin wave amplitudes. Following Suhl, one may obtain working equations for the spin wave instability analysis by retaining only linear terms in the a_k and a_{-k}^* amplitudes and terms up to second order in a_0 and a_0^*. This procedure is valid if the condition $|a_k| \ll |a_0| \ll 1$ is satisfied. A fairly tedious algebraic analysis yields general spin wave amplitude equations given by

$$-\mathrm{i}\dot{a}_k = (A_k + C_k) a_k + (B_k + D_k) a_{-k}^* + |\gamma| h_z a_k \tag{29}$$

and the companion complex conjugate equation with $\mathbf{k}$ replaced by $-\mathbf{k}$. The coefficients A_k, B_k, C_k, and D_k are given by

$$A_k = |\gamma| [H_{\mathrm{eff}}^{\mathrm{S}} + Dk^2 - M_{\mathrm{s}}(A_{xx} + A_{yy})/2] + \omega_M (\sin^2 \theta_k)/2, \tag{30}$$

$$B_k = \omega_M \sin^2 \theta_k \exp(2\mathrm{i}\varphi_k)/2 - |\gamma| M_{\mathrm{s}} (A_{xx} - A_{yy} + 2\mathrm{i} A_{xy})/2, \tag{31}$$

$$
\begin{aligned}
C_k = & -\omega_M \sin 2\theta_k [a_0 \exp(-\mathrm{i}\varphi_k) + a_0^* \exp(\mathrm{i}\varphi_k)]/4 \\
& + [|\gamma| M_s (A_{zx} - \mathrm{i}A_{zy}) - \omega_M (\tilde{N}_{zx} - \mathrm{i}\tilde{N}_{zy})] a_0/2 \\
& + [|\gamma| M_s (A_{zx} + \mathrm{i}A_{zy}) - \omega_M (\tilde{N}_{zx} + \mathrm{i}\tilde{N}_{zy})] a_0^*/2 \\
& + |\gamma| h_\perp a_0^*/2 + |\gamma| M_0 (A_{xx} + A_{yy} - 2A_{zz}) \\
& \times a_0 a_0^*/4 + \omega_M (2\tilde{N}_{zz} - \tilde{N}_{xx} - \tilde{N}_{yy} \\
& + 3\cos^2\theta_k - 1) a_0 a_0^*/4 - \omega_M (\tilde{N}_{xx} + 2\mathrm{i}\tilde{N}_{xy} \\
& - \tilde{N}_{yy}) a_0^* a_0^*/4, \qquad (32)
\end{aligned}
$$

and

$$
\begin{aligned}
D_k = & [-\omega_M \sin 2\theta_k \exp(\mathrm{i}\varphi_k)/2 \\
& + |\gamma| M_s (A_{zx} + \mathrm{i}A_{zy})] a_0 \\
& + |\gamma| h_\perp a_0 - \omega_M \sin^2\theta_k \exp(2\mathrm{i}\varphi_k) a_0 a_0^*/4 \\
& - \omega_M (\tilde{N}_{xx} + 2\mathrm{i}\tilde{N}_{xy} - \tilde{N}_{yy}) a_0 a_0^*/4 \\
& + |\gamma| M_s (A_{xx} + 2\mathrm{i}A_{xy} - A_{yy}) a_0 a_0^*/4 \\
& + \omega_M (2\cos^2\theta_k - \tilde{N}_{xx} - \tilde{N}_{yy}) a_0 a_0^*/4 \\
& + |\gamma| (Dk^2 - M_s A_{zz}) a_0 a_0/2. \qquad (33)
\end{aligned}
$$

In the above expressions, θ_k and φ_k are the standard polar and azimuthal angles of the spin wave wave vector in the (x, y, z) precession frame, respectively, $\omega_M = 4\pi|\gamma| M_s$ expresses the magnetic induction $4\pi M_s$ in frequency units, $\tilde{N}_{ij} = N_{ij} - A_{ij}/4\pi$ correspond to reduced effective demagnetizing DC magnetizing tensor elements, and $h_\perp = h_x + ih_y$ expresses the transverse components of the external microwave field **h** in the same scalar complex form used above for the transverse magnetization and dynamic effective field.

Eq. (29) and its companion equation are the working equations for the spin wave dispersion and for the first- and second-order spin wave instability threshold analysis. The linear A_k and B_k terms, considered alone, give the spin wave dispersion. The A_k and B_k coefficients contain only materials parameters and the spin wave wave vector **k**. The non-linear C_k, D_k, and h_z terms lead to spin wave instability. The C_k and D_k coefficients involve the external microwave field both explicitly and through uniform mode a_0 factors.

The details of the procedure for spin wave instability analysis are well established [2,23]. One first uses the Holstein Primakoff (HP) transformation [23] to diagonalize Eq. (29) with only the linear A_k and B_k terms taken into account and obtains the dispersion. In terms of the parameters established above, this is accomplished through a transformation from a_k and a_{-k}^* to a new set of spin wave amplitudes b_k and b_{-k}^* according to

$$a_k = \lambda_k b_k - \mu_k b_{-k}^* \qquad (34)$$

and

$$a_{-k}^* = \lambda_k b_{-k}^* - \mu_k^* b_k \qquad (35)$$

with transformation coefficients given by

$$\lambda_k = \sqrt{\frac{A_k + \omega_k}{2\omega_k}} \qquad (36)$$

and

$$\mu_k = \sqrt{\frac{A_k - \omega_k}{2\omega_k}} \, \frac{B_k}{|B_k|}. \qquad (37)$$

The ω_k term in Eqs. (36) and (37) is the bulk spin wave frequency

$$\omega_k = \sqrt{A_k^2 - |B_k|^2}. \qquad (38)$$

The spin wave dispersion relation of Eq. (38) gives rise to the usual spin wave band of allowed excitations discussed by Sparks [23] and others. The present result, when all anisotropy terms are included, gives a general spin wave dispersion for anisotropic ferrites. Special cases have been considered in Refs. [12,13,24].

Through this HP transformation, the linear terms in Eq. (29) yield a simple harmonic oscillator response equation of the form $-\mathrm{i}\mathrm{d}b_k/\mathrm{d}t = \omega_k b_k$. The key step in the instability analysis is now to apply the *same* HP transformation defined above to the *non-linear* as well as the *linear* terms in Eq. (29). This step changes Eq. (29) to the form

$$-\mathrm{i}\dot{b}_k = \omega_k b_k + F_k b_k + G_k b_{-k}^*, \qquad (39)$$

with corresponding changes to the companion equation. The F_k and G_k functions are given by

$$
\begin{aligned}
F_k = & \lambda_k^2 (|\gamma| h_z + C_k) + |\mu_k^2| (|\gamma| h_z^* + C_k^*) \\
& - \lambda_k (D_k \mu_k^* + \mu_k D_k^*) \qquad (40)
\end{aligned}
$$

and

$$
\begin{aligned}
G_k = & \lambda_k^2 D_k + \mu_k^2 D_k^* - \lambda_k \mu_k (|\gamma| h_z + |\gamma| h_z^* \\
& + C_k + C_k^*). \qquad (41)
\end{aligned}
$$

Note that all terms in both F_k and G_k terms in Eq. (39) contain factors related to the microwave driving field, either directly in terms of explicit components of **h** or indirectly in terms of the uniform mode a_0 factors. Refer to Eqs. (32) and (33).

The transformation of the non-linear terms in Eq. (29) modifies $-\mathrm{i}\mathrm{d}b_k/\mathrm{d}t = \omega_k b_k$ equation in two important ways. First, the F_k factor adds a complicated modulation to the spin wave frequency. Second, the coefficient G_k provides a coupling between the b_k and b^*_{-k} modes. Parallel comments apply to the companion equation. These modifications relate to the well-known problem of coupled harmonic oscillators [22]. A modulation in the coupling coefficient can lead to the transfer of energy from the source of the modulation to the coupled oscillators. In the present case, the G_k factor represents this coupling and the energy which is coupled into the b_k and b^*_{-k} modes is the source of spin wave instability in the Suhl analysis. Above some critical microwave field amplitude, one finds an abrupt increase in the b_k and b^*_{-k} amplitudes. The F_k factor leads only to a small modulation in the spin wave frequency. For this reason, the F_k modulation term is omitted from the Suhl instability analysis.

It is important to realize that the terms in Eq. (41) contain harmonic factors of the form $\mathrm{e}^{\mathrm{i}n\omega t}$ with n values from -2 to 2, including zero. In order to make these harmonic terms explicit, G_k may be cast in the form [2]

$$G_k = \sum_{-2}^{2} G_k^{(n)} \mathrm{e}^{\mathrm{i}n\omega t}. \tag{42}$$

As the analysis will show, the $n = 1$ and 2 terms lead to first-order instability processes for spin waves at $\omega_k = \omega/2$ and second-order processes at $\omega_k = \omega$, respectively. The label "first order" relates to the fact that the $\mathrm{e}^{\mathrm{i}\omega t}$ terms are associated with h and a_0 factors to the first power. The term "second order" relates to combinations of these factors to the second power.

The next step in the analysis is to consider the b_k equation of motion from Eq. (39) with F_k set to zero and G_k replaced by one n term only from Eq. (42). It may be easily shown that the corresponding coupled equations of motion for b_k and b^*_{-k},

$$-\mathrm{i}\dot{b}_k = \omega_k b_k + G_k^{(n)} b^*_{-k} \mathrm{e}^{\mathrm{i}n\omega t} \tag{43}$$

and

$$-\mathrm{i}\dot{b}^*_{-k} = \omega_k b^*_{-k} + (G_{-k}^{(n)})^* b_k \mathrm{e}^{-\mathrm{i}n\omega t} \tag{44}$$

have solutions which may be written in the form

$$b_k = b^n_{k0} \mathrm{e}^{\mathrm{i}n\omega t/2}. \tag{45}$$

One then examines the conditions which yield unstable growth in the b^n_{k0} amplitudes.

The next step in the procedure is to introduce relaxation for the b_k amplitudes. Following Schlömann [2], such relaxation is included through the replacement $\omega_k \to \omega_k + i\eta_k$ in Eqs. (43) and (44), where η_k corresponds to a spin wave relaxation rate. This modification in Eqs. (43) and (44), along with the substitution from Eq. (45), gives a second-order differential equation for b^n_{k0},

$$\left[\frac{\mathrm{d}^2}{\mathrm{d}t^2} + 2\eta_k \frac{\mathrm{d}^2}{\mathrm{d}t} - |G_k^{(n)}|^2 + \left(\omega_k - \frac{n\omega}{2}\right)^2 + \eta_k^2\right] b^n_{k0} = 0. \tag{46}$$

Eq. (46) has a simple algebraic solution of the form $b^n_{k0} \propto \mathrm{e}^{\kappa t}$ with κ given by

$$\kappa = -\eta_k + \sqrt{|G_k^{(n)}|^2 - (\omega_k - n\omega/2)^2}. \tag{47}$$

The increment parameter κ determines the instability condition for the b_k amplitudes. Keep in mind that b_k correspond to particular pairs of spin waves defined by ω_k and **k**.

For $\kappa > 0$, b^n_{k0} will grow exponentially with time. This corresponds to unstable spin wave growth. For a given index n, therefore, spin wave instability can occur only if $G_k^{(n)}$ satisfies the condition

$$|G_k^{(n)}|^2 > (\omega_k - n\omega/2)^2 + \eta_k^2. \tag{48}$$

Keep in mind that the control parameter throughout the entire instability analysis is the G_k coupling coefficient. Recall also that G_k ultimately involves terms which scale with the microwave field and is controlled by the microwave power level at the sample. An equal sign in place of " > " in Eq. (48) will define the spin wave instability threshold

microwave field for a given index n and the corresponding spin wave pair at ω_k and $\mathbf{k}$.

Measurements of the threshold microwave field amplitude for spin wave instability are often used in conjunction with Eq. (48) to obtain empirical values for the spin wave relaxation rate η_k. This relaxation rate is often expressed in terms of an equivalent spin wave linewidth

$$\Delta H_k = 2\eta_k/|\gamma|. \tag{49}$$

Such a spin wave linewidth parameter is useful for comparison with ferromagnetic resonance linewidths in the ferrite sample.

Eq. (48) constitutes the working equation for the determination of the spin wave instability threshold microwave field amplitude $h_{\rm crit}$ for a given material, sample shape and orientation, static field, and microwave field polarization. The procedure is to examine all possible thresholds based on Eq. (48) and the available spin waves at a given ω_k, identify that particular $(\omega_k, \mathbf{k})$ mode pair with the lowest threshold as the critical mode, and assign that minimum threshold value as $h_{\rm crit}$.

The first step in this procedure is to note that the relaxation rate η_k is typically much less than ω_k and the minimum threshold will be obtained only for $\omega_k - n\omega/2 = 0$. This condition can be satisfied only for $n = 1$, with ω_k *equal to one-half* the pumping frequency ω, or for $n = 2$, with ω_k *equal to* ω. These two cases correspond to the first- and second-order processes introduced in the discussion following Eq. (42) and the expansion of the general G_k function into harmonic terms.

Under these conditions, the working equation for spin wave instability threshold determinations becomes $|G_k^{(n)}| = \eta_k$ with $n = 1$ or 2, only. For $n = 1$, $|G_k^{(1)}| = \eta_k$ gives the spin wave specific threshold $h_c^{(1)}(\omega_k = \omega/2, \mathbf{k})$ for first-order processes. For $n = 2$, $|G_k^{(2)}| = \eta_k$ gives the spin wave specific threshold $h_c^{(2)}(\omega_k = \omega, \mathbf{k})$ for second-order processes. The second and final step in the procedure to obtain $h_{\rm crit}$ is to seek the minimum $h_c^{(1)}$ or $h_c^{(2)}$ over all available spin wave states at $\omega_k = \omega/2$ or $\omega_k = \omega$, respectively.

The immediate task at hand, therefore, is to examine the various harmonic terms in G_k and obtain explicit expression for $G_k^{(1)}$ and $G_k^{(2)}$. Inspection of Eqs. (32), (33) and (41) shows that all harmonic time dependencies for G_k are contained in the scalar complex uniform mode amplitude a_0 and the z-component of the applied microwave field h_z. The next section will introduce a general microwave pumping field $\mathbf{h}$ and establish working equations for the complex uniform mode amplitude a_0. Section 6 will then develop explicit working equations for the $h_{\rm crit}$ threshold for first- and second-order processes.

5. Pumping field and uniform mode response

The applied microwave field $\mathbf{h}(t)$ is taken to be uniform over the ellipsoidal sample and with a general polarization. The components of this pumping field in the precession frame may be written as

$$\begin{aligned} h_x(t) &= h_0\alpha_x \cos(\omega t + \delta_x) \\ &= h_0\alpha_x[e^{i(\omega t+\delta_x)} + e^{-i(\omega t+\delta_x)}]/2, \end{aligned} \tag{50}$$

$$\begin{aligned} h_y(t) &= h_0\alpha_y \cos(\omega t + \delta_y) \\ &= h_0\alpha_y[e^{i(\omega t+\delta_y)} + e^{-i(\omega t+\delta_y)}]/2 \end{aligned} \tag{51}$$

and

$$\begin{aligned} h_z(t) &= h_0\alpha_z \cos\omega t \\ &= h_0\alpha_z[e^{i\omega t} + e^{-i\omega t}]/2. \end{aligned} \tag{52}$$

The h_0 parameter serves to identify the amplitude of the pumping field. The relative amplitude parameters α_x, α_y, and α_z, and the phase parameters δ_x and δ_y define the specific components of the pumping field in the (x, y, z) precession frame. The above form for $\mathbf{h}(t)$ is the same as in Ref. [12].

The above uniform pumping field produces a uniform mode response $\mathbf{m}_0$. The undamped response may be evaluated from the torque equation, Eq. (25), with only linear terms in the dynamic variables taken into account. It will also be necessary to include the effects of damping, particularly for situations when one is operating close to ferromagnetic resonance. This will be accomplished by a complex frequency substitution technique. The end result is a set of equations for the complex uniform mode amplitude a_0.

Based on the above driving fields, one may obtain the undamped uniform mode response

form the x and y components of the torque equation, Eq. (25), with only linear terms in the components of $\mathbf{h}$ and $\mathbf{m}$ included. For this analysis, $\mathbf{M}$ is taken as $M_s\hat{\mathbf{z}} + \mathbf{m}_0$ only, with all $\mathbf{k} \neq 0$ terms ignored, and $\mathbf{H}_{\text{eff}}$ is taken as

$$\mathbf{H}_{\text{eff}} = H_{\text{eff}}^{S}\hat{\mathbf{z}} - 4\pi\tilde{\mathbf{N}}\mathbf{m}_0 + \mathbf{h}. \tag{53}$$

Eq. (25) may now be cast in the same form as Eq. (26) with the $h_{\text{eff},z}$ and m_z terms omitted and $h_{\text{eff}+}$ constructed from the x and y components of $\mathbf{h} - 4\pi\tilde{\mathbf{N}}\mathbf{m}_0$ only. The substitutions $m_+ = a_0 M_s$ and $m_- = a_0^* M_s$ then yield coupled equations for a_0 and a_0^* given by

$$-\mathrm{i}\dot{a}_0 = |\gamma| H_{\text{eff}}^{S} a_0 - |\gamma| h_\perp + \omega_M[(\tilde{N}_{xx} + \tilde{N}_{yy})a_0 + (\tilde{N}_{xx} + 2\mathrm{i}\tilde{N}_{xy} - \tilde{N}_{yy})a_0^*]/2 \tag{54}$$

and the companion complex conjugate. The solution of these coupled equations gives the complex uniform mode amplitude a_0 as

$$a_0(t) = |\gamma| h_0[q_{L0}\exp(\mathrm{i}\omega t) + q_{A0}\exp(-\mathrm{i}\omega t)]/2. \tag{55}$$

The q_{L0} and q_{A0} factors are given by

$$q_{L0} = \frac{(\omega_y + \omega - \mathrm{i}\omega_{xy})\alpha_x \mathrm{e}^{\mathrm{i}\delta_x} + \mathrm{i}(\omega_x + \omega + \mathrm{i}\omega_{xy})\alpha_y \mathrm{e}^{\mathrm{i}\delta_y}}{\omega_0^2 - \omega^2} \tag{56}$$

and

$$q_{A0} = \frac{(\omega_y - \omega - \mathrm{i}\omega_{xy})\alpha_x \mathrm{e}^{-\mathrm{i}\delta_x} + \mathrm{i}(\omega_x - \omega + \mathrm{i}\omega_{xy})\alpha_y \mathrm{e}^{-\mathrm{i}\delta_y}}{\omega_0^2 - \omega^2}. \tag{57}$$

The frequency parameters ω_x, ω_y and ω_{xy} are given by

$$\omega_x = |\gamma| H_{\text{eff}}^{S} + \omega_M \tilde{N}_{xx}, \tag{58}$$

$$\omega_y = |\gamma| H_{\text{eff}}^{S} + \omega_M \tilde{N}_{yy} \tag{59}$$

and

$$\omega_0 = \omega_M \tilde{N}_{xy}. \tag{60}$$

The ω_0 frequency parameter corresponds to the ferromagnetic resonance (FMR) frequency and is given by

$$\omega_{xy} = \sqrt{\omega_x \omega_y - \omega_{xy}^2}. \tag{61}$$

The $|\gamma| h_0 q_{L0}/2$ and $|\gamma| h_0 q_{A0}/2$ multipliers in Eq. (55) represent the Larmor and anti-Larmor amplitudes for the uniform mode. These amplitudes scale linearly with the pumping field amplitude h_0.

Note the singularities in the a_0 response in Eqs. (55)–(57) in the limit $\omega \to \omega_0$. This is due to the neglect of damping. Damping must be included in the analysis in order to describe properly the a_0 response, particularly when the pumping frequency ω is close to the FMR frequency ω_0. The effect of uniform mode damping can have an important effect on the instability analysis, especially for second-order processes.

There are various ways in which damping may be included in the uniform mode response [22,23]. In the previous section, spin wave damping was taken into account through a complex frequency substitution, $\omega_k \to \omega_k + \mathrm{i}\eta_k$. A similar procedure will be followed here for the uniform mode frequency [13]. This substitution may be written as

$$\omega_k \to \omega_0 + \mathrm{i}\eta_0, \tag{62}$$

where η_0 is the uniform mode relaxation rate. The applicable η_0 at ferromagnetic resonance is related to the FMR field swept linewidth ΔH_0 according to

$$\eta_0 = \frac{1}{2}\frac{\partial\omega_0}{\partial H_{\text{ext}}}\Delta H_0. \tag{63}$$

The formalism developed above provides working equations for the uniform mode amplitude a_0 for a general pumping field applied to an ellipsoidal sample with a general anisotropy. The form of Eq. (55) separates out of the specific $\mathrm{e}^{\pm\mathrm{i}\omega t}$ harmonic time dependencies for the Larmor and anti-Larmor response terms in a_0. The incorporation of the various harmonic terms in a_0 and $\mathbf{h}$ into in the general G_k expression of Eq. (41) then allows one to construct explicit expressions for $G_k^{(1)}$ and $G_k^{(2)}$. The final step in the formal analysis is to set up working equations for the spin wave instability threshold and critical modes.

6. Critical fields and critical modes

This section serves two functions. First, it establishes simple working equations for $h_c^{(1)}$ and $h_c^{(2)}$, the specific threshold fields for a general

spin wave pair with wave vectors of $\pm\mathbf{k}$ and frequency $\omega_k = \omega/2$ or ω. Second, the minimization procedure to obtain actual first- and second-order $h_{\rm crit}$ values from $h_{\rm c}^{(1)}$ and $h_{\rm c}^{(2)}$ is outlined. Section 7 will then present an example calculation to demonstrate the practical use of the theory.

Consider first-order processes. A convenient working equation for the threshold field $h_{\rm c}^{(1)}(\omega_k = \omega/2, \mathbf{k})$ may be obtained by writing $h_{\rm c}^{(1)}$ as the ratio of the spin wave linewidth ΔH_k and a dimensionless coupling parameter $Y_k^{(1)}$ according to

$$h_{\rm c}^{(1)} = \frac{\Delta H_k}{|Y_k^{(1)}|}. \tag{64}$$

The development in Sections 4 and 5 yields a $Y_k^{(1)}$ function which may be written as

$$\begin{aligned} Y_k^{(1)} = {} & [\lambda_k^2 q_{L0} d_k + \mu_k^2 q_{A0}^* d_k^* \\ & - \lambda_k \mu_k (2\alpha_z + q_{L0} c_k + q_{A0}^* c_k^*] \end{aligned} \tag{65}$$

with the coefficients c_k and d_k given by

$$\begin{aligned} c_k = {} & -\omega_M(\sin 2\theta_k e^{-i\varphi_k}/2 + \tilde{N}_{zx} - i\tilde{N}_{zy}) \\ & + |\gamma| M_s (A_{zx} - iA_{zy}) \end{aligned} \tag{66}$$

and

$$\begin{aligned} d_k = {} & -\omega_M \sin 2\theta_k e^{i\varphi_k}/2 \\ & + |\gamma| M_s (A_{zx} + iA_{zy}). \end{aligned} \tag{67}$$

Note that the λ_k, μ_k, and a_z parameters are dimensionless, q_{L0} and q_{A0} have dimensions of inverse frequency, and c_k and d_k have dimensions of frequency. For isotropic ellipsoids of revolution and pure transverse Larmor or parallel pumping, $|Y_k^{(1)}|$ reduces to the first-order threshold limiting case expression obtained by Suhl and Schlömann.

In a similar way, the threshold field $h_{\rm c}^{(2)}(\omega_k = \omega, \mathbf{k})$ for second-order processes may be written in the form

$$h_{\rm c}^{(2)} = 2\sqrt{\frac{4\pi M_s \Delta H_k}{|Y_k^{(2)}|}}, \tag{68}$$

where $Y_k^{(2)}$ is a dimensionless coupling factor defined by

$$\begin{aligned} Y_k^{(2)} = {} & \omega_M \lambda_k^2 [q_{L0}^2 f_k + q_{L0} q_{A0}^* g_k \\ & + q_{L0}(\alpha_x e^{i\delta_x} + i\alpha_y e^{i\delta_y})] \\ & + \omega_M \mu_k^2 [q_{A0}^{*2} f_k + q_{L0} q_{A0}^* g_k^* \\ & + q_{A0}^*(\alpha_x e^{i\delta_x} - i\alpha_y e^{i\delta_y})] \\ & - \omega_M \lambda_k \mu_k [2 r_k q_{L0} q_{A0}^* \\ & + s q_{L0}^2 + s^* q_{A0}^{*2} \\ & + q_{A0}^*(\alpha_x e^{i\delta_x} + i\alpha_y e^{i\delta_y}) \\ & + q_{L0}(\alpha_x e^{i\delta_x} - i\alpha_y e^{i\delta_y})]. \end{aligned} \tag{69}$$

The as yet undefined coefficient are given by

$$\begin{aligned} f_k = {} & |\gamma| D k^2 + \omega_M \cos^2\theta_k - |\gamma| M_s A_{zz} \\ & - \omega_M(\tilde{N}_{xx} + \tilde{N}_{yy})/2, \end{aligned} \tag{70}$$

$$\begin{aligned} g_k = {} & -\omega_M(\tilde{N}_{xx} + 2i\tilde{N}_{xy} - \tilde{N}_{yy} + \sin^2\theta_k e^{2i\phi_k})/2 \\ & + |\gamma| M_s (A_{xx} + 2iA_{yx} - A_{yy})/2, \end{aligned} \tag{71}$$

$$\begin{aligned} r_k = {} & \omega_M \cos^2\theta_k + \omega_M \tilde{N}_{zz} + |\gamma| M_s (A_{xx} + A_{yy})/2 \\ & - |\gamma| M_s A_{zz} - \omega_M(\tilde{N}_{xx} + \tilde{N}_{yy} + \sin^2\theta_k)/2 \end{aligned} \tag{72}$$

and

$$s = -\omega_M(\tilde{N}_{xx} - 2i\tilde{N}_{xy} - \tilde{N}_{yy})/2. \tag{73}$$

The f_k, g_k, r_k, and s have dimensions of frequency. For isotropic ellipsoids of revolution and pure transverse Larmor pumping, $|Y_k^{(2)}|$ reduces to the simple limiting case second-order threshold expression obtained by Suhl.

The results contained in Eqs. (64)–(73) give the first completely general formulation of the first- and second-order threshold problem for a general anisotropy, a general microwave field configuration, a general ellipsoidal sample shape, and a non-collinear magnetization-field condition. This general result follows from application of the traditional spin wave instability analysis of Suhl and Schlömann almost verbatim, but with an effective field formulation based on the free energy considerations outlined in Section 2 and the precession frame transformation procedure of Section 3.

All that remains is to examine the range of available spin wave wave vectors at $\omega_k = \omega/2$ for

first-order processes or at $\omega_k = \omega$ for second-order processes, and determine the lowest value of $h_c^{(1)}(\omega_k = \omega/2, \mathbf{k})$ or $h_c^{(2)}(\omega_k = \omega, \mathbf{k})$ for the available states, and obtain h_{crit}. The hardest part of this analysis often turns out to be in setting up the minimization procedure over the available spin wave $\mathbf{k}$ states. This can be particularly challenging when the anisotropy has a significant effect on the spin wave dispersion relation of Eq. (38). The details of such minimization can be cogently discussed only within the context of a specific material and geometry. A demonstration example is given in the next section.

As emphasized above, the formulation given here is general. The specific working equations, however, have been set up in a way which facilitates the inspection of the results in special cases which correspond to the original results of Suhl and Schlömann. For parallel pumping in isotropic ferrites, for example, the first-order threshold equations given above reduce to

$$|Y_k^{(1)}| = 2\lambda_k|\mu_k|a_z = |B_k|/\omega_k = \omega_m \sin^2\theta_k/\omega. \quad (74)$$

This $|Y_k^{(1)}|$, in combination with Eq. (64) yields the well-known parallel pumping threshold $h_{crit} = \omega\Delta H_k/\omega_M$ with the critical modes at $\theta_k = 90^\circ$ [3].

7. Demonstration calculation—first–order thresholds for an easy plane ferrite disk

This section supplements the previous general development by way of a specific example. The system considered is a thin disk with an easy plane anisotropy which coincides with the disk plane. The numerical evaluations are done for parameters applicable to Zn–Y, a Y-type hexagonal ferrite with planar anisotropy [20]. Only first-order processes are considered. The results will be presented in the form of curves of the spin wave instability threshold field h_{crit} as a function of H_{ext}, along with curves of the corresponding critical mode spin wave wave number k and polar angle θ_k as a function of H_{ext}.

The geometry of the problem is shown in Fig. 3. The disk is in the $X-Y$ plane of the (X, Y, Z) laboratory frame. The $X-Y$ plane is also the easy plane for the Zn–Y sample, and the Z-axis

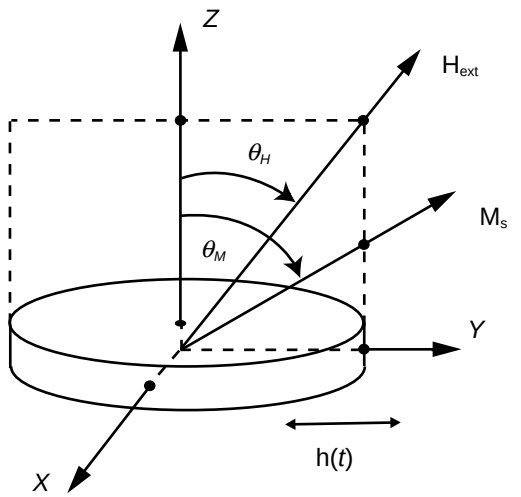

Fig. 3. Geometry for the easy plane disk threshold analysis. The disk is in the $X-Y$ plane of the (X, Y, Z) laboratory frame. The external static field $\mathbf{H}_{ext}$ is in the $Y-Z$ plane at an angle θ_H relative to Z. The static magnetization $\mathbf{M}_s$ is in the $Y-Z$ plane at an angle θ_M relative to Z. The linearly polarized microwave field $\mathbf{h}(t)$ is along Y.

corresponds to the hexagonal c-axis. The field $\mathbf{H}_{ext}$ is in the $Y-Z$ plane and at an angle θ_H to the Z-axis. The magnetization $\mathbf{M}_s$ is in the $Y-Z$ plane and at an angle θ_M to the Z-axis. The linearly polarized microwave field $\mathbf{h}(t)$ is along Y-axis. The figure shows a disk of finite extent and non-zero thickness. For simplicity, the disk demagnetizing factors will be set at $N_X = N_Y = 0$ and $N_Z = 1$. This corresponds to a disk diameter which is very large compared to the thickness. The microwave field $\mathbf{h}(t)$ will be taken to be uniform over the disk.

The easy plane anisotropy may be characterized in terms of an energy density function of the form

$$F_A = -K_U \cos^2\theta_M = -K_U M_Z^2/M_s^2, \quad (75)$$

where K_U is an anisotropy parameter. For this anisotropy, the anisotropy field $\mathbf{H}_A$ defined in Eq. (5) has only one non-zero component, $H_{A,Z} = H_A \cos\theta_M$, where $H_A = 2K_U/M_s$ is a scalar anisotropy field parameter. For easy-plane Zn–Y, K_U and H_A are negative.

For planar anisotropy and the geometry of Fig. 3, it is clear that M_s will lie in the plane defined by $\mathbf{H}_{ext}$ and the Z-axis, with the azimuthal angles φ_M and φ_H in Fig. 1 equal to $\pi/2$. For the analysis below, the field H_{ext} and the polar field

angle θ_H will be the control parameters. As either of these field parameters is changed, the polar angle θ_M will also change. For each $(H_{\rm ext}, \theta_H)$ combination, θ_M will be obtained from the static equilibrium condition of Eq. (19). For this example, Eq. (19) reduces to

$$H_{\rm ext}\sin(\theta_H - \theta_M) = (H_{\rm A} - 4\pi M_{\rm s})\sin(2\theta_M)/2. \quad (76)$$

The equilibrium θ_M value then establishes the specific precession frame geometry and the associated tensor components of the demagnetizing tensor $\mathbf{N}$ and the anisotropy tensor $\mathbf{A}$ in the precession frame. The components of $\mathbf{N}$ follow from Eqs. (12)–(17). For the geometry of Fig. 3, there are only two non-zero $\mathbf{N}$ components, $N_{xx} = N_Z \sin^2\theta_M$ and $N_{zz} = N_Z \cos^2\theta_M$. The components of the anisotropy tensor $\mathbf{A}$ follow from Eqs. (7), (11) and (18). For an anisotropy energy function $F_{\rm A}$ of the form in Eq. (75) and a θ_M which satisfies the static equilibrium condition for a given $(H_{\rm ext}, \theta_H)$ pair, the laboratory frame anisotropy tensor $\mathbf{A}'$ defined by Eq. (7) has only one non-zero component, $A'_{zz} = H_{\rm A}/M_{\rm s}$. The corresponding non-zero components of the precession frame anisotropy tensor $\mathbf{A}$ are $A_{xx} = H_{\rm A}\sin^2\theta_M/M_{\rm s}$ and $A_{zz} = H_{\rm A}\cos^2\theta_M/M_{\rm s}$.

For the threshold evaluations, the microwave field is taken to have the explicit form $\mathbf{h}(t) = h_0\cos(\omega t)\hat{\mathbf{Y}}$. The corresponding microwave field in the precession frame is then given by Eqs. (50)–(52) with $\alpha_x = \cos\theta_M$, $\alpha_z = \sin\theta_M$, and the remaining parameters α_y, δ_x, and δ_y set to zero.

Based on the above expressions, one can now construct explicit formulae for the static effective field $H^{\rm S}_{\rm eff}$, the spin wave dispersion relation $\omega_k(k, \theta_k, \varphi_k)$, the uniform mode response functions q_{L0} and q_{A0}, and the first-order coupling parameter $Y^{(1)}_k$. Based on these formulae, one may set up a suitable scan over available spin wave states at $\omega_k = \omega/2$, and determine the minimum threshold $h_{\rm crit}$ and the corresponding (k, θ_k, φ_k) critical mode parameters for first-order processes. If desired, one could follow a similar procedure for second-order processes, based on $Y^{(2)}_k$ and a scan over available spin wave states at $\omega_k = \omega$.

The most challenging step in the above threshold calculation procedure is the set up of an appropriate scan over the available spin wave states. In the general case, one may construct a suitable scan in a purely mathematical way, based on the full ranges of $0-\pi$ for θ_k and $0-2\pi$ for φ_k, and the requirement that k be limited to real values. In any event, one simply calculates the threshold $h^{(1)}_{\rm c}(\omega_k = \omega/2, \mathbf{k})$ or $h^{(2)}_{\rm c}(\omega_k = \omega, \mathbf{k})$ for the full range of allowed $\mathbf{k}$ values, picks the minimum threshold value as $h_{\rm crit}$ and the corresponding (k, θ_k, φ_k) critical mode. Note, that $+\mathbf{k}$ and $-\mathbf{k}$ spin waves correspond to (k, θ_k, φ_k) and $(k, \pi - \theta_k, \pi + \varphi_k)$ spin waves, respectively, and these modes give the same threshold $h_{\rm crit}$. For convenience, only critical modes with θ_k in the range $0-\pi/2$ were taken into account.

The above procedure was used to obtain explicit numerical values for $h^{(1)}_{\rm c}$ over the full range of available spin wave states and then evaluate $h_{\rm crit}$. This was done for a range of applied fields and field angles. These numerical results were then used to construct curves of $h_{\rm crit}$ vs. $H_{\rm ext}$ with θ_H as a control parameter. For these evaluations, $H_{\rm A}$ was set at -9.0 kOe, $4\pi M_{\rm S}$ was set at 2800 G, $|\gamma|$ was set to the free electron value of 1.76×10^7 rad/s Oe, $\omega/2\pi$ was set at 9 GHz, the exchange constant D was set to 5×10^{-9} Oe cm^2/rad^2, and ΔH_k was set at 1 Oe. The chosen D value is for yttrium iron garnet. There is no reported D value in the literature for Zn–Y.

Fig. 4 shows selected results from the numerical evaluations. Graph (a) gives $h_{\rm crit}$ vs. $H_{\rm ext}$ for θ_H values of 90°, 10°, and 5°. Graphs (b) and (c) give corresponding results on the critical mode spin wave number k and polar angle θ_k as a function of $H_{\rm ext}$. For $\theta_H = 90°$, the critical mode azimuthal spin wave angle φ_k was double valued at 0° or 180°. For any θ_H value below 90°, the minimum threshold critical mode φ_k was *single valued* at 180°.

One aspect of Fig. 4(a) and (c) requires additional comment. In graph (a), the $h_{\rm crit}$ curve for $\theta_H = 90°$ sticks at a constant value as long as the critical mode k value is non-zero. This corresponds to the flat part of the curve in (a) for $\theta_H = 90°$ and $H_{\rm ext}$ below about 0.25 kOe. The other $h_{\rm crit}$ vs. $H_{\rm ext}$ curves for $\theta_H = 10°$ and 5° in graph (a) start out at the same $h_{\rm crit}$ value as for $H_{\rm ext} = 0$, but then increase slightly as $H_{\rm ext}$ is increased. The fact that the initial part of the $\theta_H = 90°$ curve in (a) is flat,

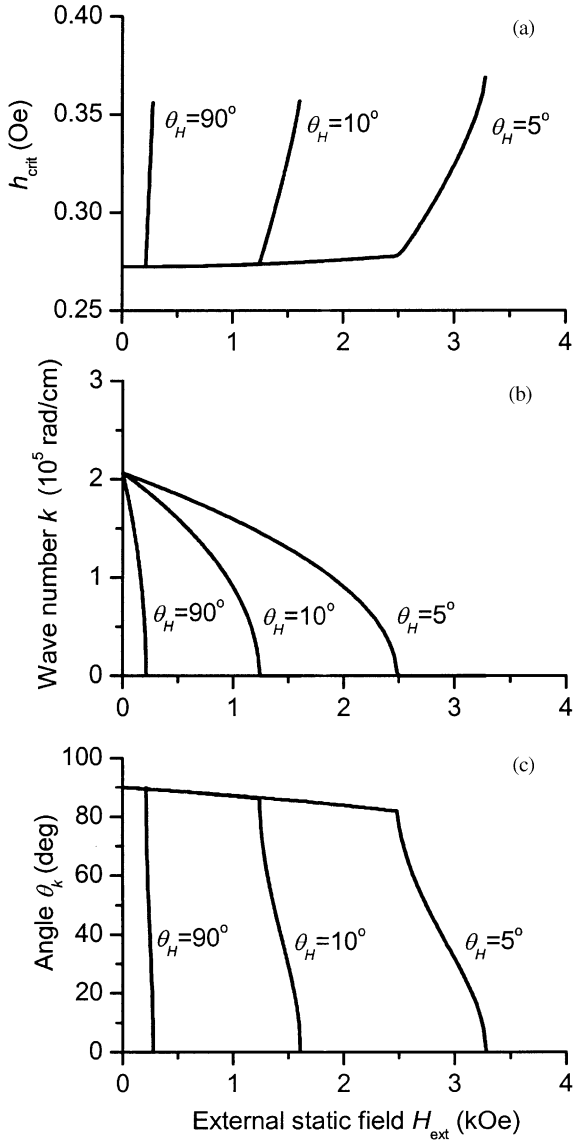

Fig. 4. Threshold and critical mode parameters as a function of the external filed H_{ext} for the easy plane disk with 9 GHz microwave excitation. The graphs show (a) first-order spin wave instability threshold field h_{crit} vs. H_{ext}, (b) critical mode spin wave wave number k vs. H_{ext}, and (c) polar spin wave propagation angle θ_k vs. H_{ext}. The graphs show results for values of θ_H, the field angle relative to the disk normal, as indicated.

while the other curves have a non-zero low field slope is not obvious from the curves.

The critical mode θ_k vs. H_{ext} response in Fig. 4(c) shows a similar effect. The curve for the critical mode θ_k vs. H_{ext} for $\theta_H = 90^\circ$ sticks at precisely 90° as long as the critical mode k is non-zero. The curves for $\theta_H = 10^\circ$ and 5° start out at $\theta_k = 90^\circ$ for $H_{ext} = 0$ but decrease slightly as H_{ext} is increased from zero. These subtle effects are related to the change in the pumping configuration when $\mathbf{M}_s$ is pulled out of the disk plane. For $\theta_H = 90^\circ$, one has a simple parallel pumping geometry. For $\theta_H \neq 90^\circ$, one has a more complicated pumping geometry with both parallel and perpendicular pumping components. These distinctions will be considered in more detail below.

These results demonstrate the power of the general theory. Consider first the left most curves in the Fig. 4 graphs for $\theta_H = 90^\circ$. As noted above, these results correspond to parallel pumping. This case, parallel pumping for an in-plane magnetized easy plane sample, corresponds to the specific problem considered by Schlömann et al. [13]. For fields below about 200 Oe, h_{crit} is constant, the critical mode k decreases, and the critical mode θ_k sticks at 90°. Above 200 Oe, there in a jump in h_{crit} and a rapid drop in the critical mode θ_k to zero over a very narrow field interval. These responses are all related to the shape of the spin wave band for this geometry and the critical mode behavior as it relates to this shape.

A perspective sketch of spin wave dispersion band for this parallel pump situation is shown in Fig. 5. The diagram is for purposes of illustration only and not to scale for the Zn–Y example considered here. The dispersion is shown for some fixed value of H_{ext}. The φ_k axis is shown for 0–90° only in order to keep the diagram uncluttered. The inset shows ω_k vs. φ_k for the range 0–180° for the top of the band at $\theta_k = 90^\circ$ and $k = 0$. An increase in H_{ext} would shift the entire band up in frequency. Two constant θ_k surfaces are indicated. The $\theta_k = 0$ surface which defines the bottom of the band is φ_k independent and curves upward with increasing k due to exchange. The $\theta_k = 90^\circ$ surface which defines the top of the band changes with φ_k. This φ_k dependence causes the warped surface evident in the figure.

Keep in mind that the first-order threshold calculation for a given H_{ext} will involve a scan over available spin wave states at $\omega_k = \omega/2$. The available modes will correspond to a particular

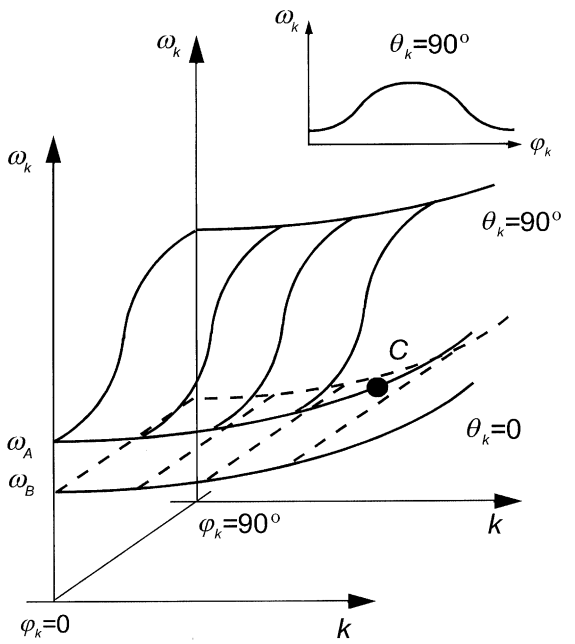

Fig. 5. Schematic bulk spin wave dispersion diagram for an easy plane disk with the static field in plane at $\theta_H = 90°$. The graph show the spin wave frequency ω_k vs. wave number k and azimuthal spin wave propagation angle φ_k for $\theta_k = 0°$ and 90°, where θ_k is the polar spin wave propagation angle. The inset shows ω_k vs. φ_k for $\theta_k = 90°$. Note that in Refs. [13,24] the coordinate system is different and $\varphi_k = 90°$ corresponds to $\varphi_k = 0°$ in this figure.

horizontal cut across the band in Fig. 5. As the field is increased, the spin wave band will move up, relative to this cut. The minimum threshold critical mode will correspond to a particular point on this cut, and the critical mode parameters will also change as the field is changed.

At very low field, the $\omega/2$ cut will be above point ω_A in Fig. 5. As shown by Fig. 4(b) and (c), the minimum threshold critical mode at $\theta_H = 90°$ for low fields has a non-zero k and $\theta_k = 90°$. As noted, this critical mode also has a φ_k of 0° or 180°. The corresponding critical mode point is labeled "C" in Fig. 5. As the field is increased, the $\omega/2$ cut remains fixed and the entire band shifts up. This causes the critical mode point to move down in k. At some point in field, point ω_A moves up to meet the $\omega/2$ cut and the critical mode k-value goes to zero. This part of the critical mode behavior corresponds to the constant part at the start of the h_{crit} vs. H_{ext} curve in Fig. 4(a) for $\theta_H = 90°$. The corresponding change in k is evident in Fig. 4(b). Note that θ_k is constant over this same field interval, as noted above and shown in Fig. 4(c). Note also that φ_k remains at 0° or 180° over this entire range.

As the field is increased further, the band continues to shift up relative to the $\omega/2$ cut. Correspondingly, the critical mode point moves from ω_A down to ω_B at the very bottom of the band, θ_k changes gradually from 90° to 0°, and φ_k remains at 0° or 180° as before. This response corresponds to the steeply rising part of the h_{crit} vs. H_{ext} curve in Fig. 4(a) for $\theta_H = 90°$, as well as the rapid drop in θ_k in graph (a). Note that at the $\omega/2 = \omega_B$ end point, the h_{crit} threshold is finite. For isotropic materials, the threshold at this band edge diverges because the limiting mode is circularly polarized. For Zn–Y, this end point mode is elliptically polarized and one obtains a non-infinite threshold. This observation was first made by Schlömann [13]. One may also note that the ellipticity causes a drastic factor-of-four reduction in the overall threshold for Zn–Y, relative to isotropic ferrite materials.

There is a fundamental reason for the critical mode response described above. In the case of parallel pumping the minimum threshold mode is always the mode with the largest spin precession ellipticity. One may use simple dipole energy arguments to show that for an $\omega/2$ cut above ω_A, the mode with the highest ellipticity sits at $\theta_k = 90°$ and 0° or 180°. When the cut falls below ω_A, the maximum ellipticity condition keeps φ_k at 0° or 180°, and θ_k is forced to decrease as ω_A and ω_B move up.

Turn now to the two sets of curves in Fig. 4 for $\theta_H \neq 90°$. These curves are completely different from the situation for $\theta_H = 90°$ in-plane field case. The reason is that as θ_H drops below 90° so that the applied field is out plane, any non-zero value of H_{ext} will pull the static magnetization out of the disk plane. This has dire consequences for (1) the pumping configuration and (2) the response of the spin wave band to changes in the applied field.

These important effects can be understood from the modified version of Fig. 3 given in Fig. 6. There are two main changes in this figure. First, the indicated axes with arrowheads are the (x, y, z)

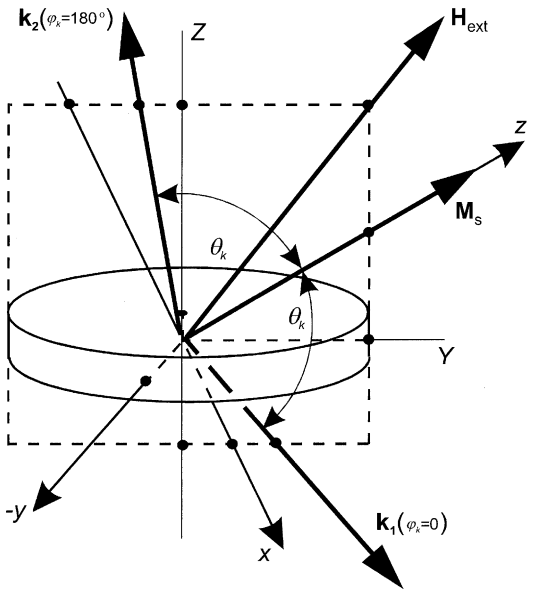

Fig. 6. Spin wave propagation geometry for an out of plane external static field H_{ext} and corresponding out of plane static magnetization M_s. The diagram shows the laboratory frame Y- and Z-axis and the precession frame $(x, -y, z)$ axes. The wave vectors $\mathbf{k}_1$ and $\mathbf{k}_2$ are for a common polar spin wave propagation angle θ_k and values of the azimuthal spin wave propagation angle φ_k of 0° and 180°, as indicated.

precession frame axes. The x-axis is in the plane of the page and the y-axis is into the page. Second, a pair of wave vectors are shown for $\varphi_k = 0°$ or 180° and a common value of θ_k, taken to be below 90°. The $\theta_k \neq 90°$ situation is chosen deliberately to demonstrate how the out-of-plane $\mathbf{H}_{ext}$ and $\mathbf{M}_s$ breaks the symmetry found for the $\theta_H = \theta_M = 90°$ situation discussed above.

When $\mathbf{H}_{ext}$ is out of plane, $\mathbf{M}_s$ will be gradually pulled out of the disk plane as H_{ext} is increased. Moreover, the modifications to the spin wave band in Fig. 5 are such that the ω_A point is pushed down in frequency for a given value of H_{ext}. The net result is a significant increase in the size of H_{ext} which is needed to raise ω_A up to the $\omega_k = \omega/2$ cut which defines the available modes for instability. The applicable equations for the present example are

$$H_{eff}^S = H_{ext}\cos(\theta_H - \theta_M) - 4\pi M_s \cos^2\theta_M + H_A \cos^2\theta_M, \quad (77)$$

the equilibrium condition of Eq. (76), and the spin wave dispersion,

$$\omega_k^2 = |\gamma|^2[H_{eff}^S + Dk^2 + H_A\cos^2\theta_M] \times [H_{eff}^S + Dk^2 + H_A\cos 2\theta_M] + |\gamma|\omega_M \sin^2\theta_k[H_{eff}^S + Dk^2 + H_A(\cos^2\theta_M - \sin^2\theta_M \sin^2\varphi_k)]. \quad (78)$$

In the $\theta_H = \theta_M = 90°$ limit, Eq. (77) reduces to $H_{eff}^S = H_{ext}$ and the spin wave band reduces to the form shown in Fig. 5. The vales of H_{ext} for which ω_A crosses $\omega/2$ for the two right most curves in Fig. 4(a) correspond to the kink points at about 1.3 and 2.5 kOe for $\theta_H = 10°$ and 5°, respectively.

The small increase in h_{crit} with H_{ext} for fields below the kink points in graph (a) of Fig. 4 for $\theta_H = 10°$ and 5°, and the corresponding weak drops in the critical mode θ_k in graph (c) curve are due to the change from pure parallel pumping to oblique pumping. Oblique pumping means that the microwave field has components both parallel and perpendicular to $\mathbf{M}_s$. This effect can be seen from Fig. 6. Keep in mind that the linearly polarized microwave field (not shown) is in the film plane and along Y, while $\mathbf{M}_s$ is tipped out of the film plane. As H_{ext} is increased, $\mathbf{M}_s$ is pulled more and more out of plane and the $\mathbf{h}$ component transverse to $\mathbf{M}_s$ increases. The increase in this transverse pumping component causes the critical mode θ_k to decrease. Note that for pure parallel pumping with $\mathbf{h}$ parallel to $\mathbf{M}_s$, the critical mode θ_k value sticks at exactly 90° even if $\mathbf{M}_s$ is pulled away from Y. In the present geometry, the microwave field direction is fixed, the out-of-plane $\mathbf{H}_{ext}$ pull $\mathbf{M}_s$ out of plane and forces the system into an oblique pumping configuration.

The change to an oblique pumping configuration has an additional effect which breaks the symmetry and shifts the critical mode response from the two equivalent φ_k propagation angles of 0° and 180° to $\varphi_k = 180°$ only. Fig. 6 shows that the out of plane $\mathbf{M}_s$ also yields a precession frame x-axis which is rotated away from the disk normal and hard c-axis in this example. The figure also shows two potential $\mathbf{k}$ vectors at $\varphi_k = 0°$ and 180°. In the case of an out of plane $\mathbf{M}_s$, it is clear that these two vectors are not equivalent. Based on the ellipticity arguments given above, one can show

that the mode with the highest ellipticity, and hence the lowest threshold, will be for the **k** which is closest to the c-axis, or the $\varphi_k = 180^\circ$ direction in the figure. The symmetry breaking effect explains, therefore, the analytical result of two equivalent critical mode propagation directions of $\varphi_k = 0^\circ$ or 180° for $\theta_H = 90^\circ$ and a single direction at $\varphi_k = 180^\circ$ for $\theta_H < 90^\circ$. Note that the symmetry in the critical mode φ_k can be broken even for oblique pumping in isotropic ferrites [4,6].

The above example demonstrates the application of the formal theory to real problems and gives specific results for first-order processes in an easy plane ferrite disk. The power of the general theory is especially evident for the oblique pumping geometry which is obtained when the static applied field is out of plane.

8. Summary and future work

The classical theory of spin wave instability in ferromagnetic insulators has been extended to include general anisotropy based on a tensor formulation of static and dynamic effective fields. The theory provides working equations for threshold calculations and critical mode determinations. The formulation is completely general and can accommodate any type of anisotropy and an arbitrary microwave field configuration. The sample shape is limited to that of a general ellipsoid in order to maintain a uniform magnetization and uniform internal static and microwave fields. The formalism includes the ability to include a general wave vector-dependent spin wave relaxation rate or linewidth. The formalism was applied to first-order processes in an easy plane ferrite disk with parameters applicable to Zn–Y hexagonal ferrite with an in-plane 9 GHz microwave pump field.

Further work is in progress to apply the theory to the analysis of experimental data on hexagonal ferrites with large anisotropy for various static and microwave field configurations. The objective of this work is to elucidate the nature of spin wave instability processes and the corresponding critical modes for complex pumping configurations in anistropic ferrite materials, and to determine the wave vector dependent spin wave linewidth in these materials.

Acknowledgements

Mark M. Scott and Dr. David Menard are acknowledged for helpful discussions. This work was supported in part by the United States Office of Naval Research, Grant N00014-94-1-0096.

References

[1] H. Suhl, J. Phys. Chem. Solids 1 (1957) 209.
[2] E. Schlömann, Raytheon Tech. Report R-48, Waltham, MA, 1959.
[3] E. Schlömann, J.J. Green, U. Milano, J. Appl. Phys. 31 (1960) 386S.
[4] Y.M. Yakovlev, Sov. Phys. Solid State 10 (1969) 1911.
[5] J.J. Green, C.E. Patton, E. Stern, J. Appl. Phys. 40 (1969) 172.
[6] C.E. Patton, J. Appl. Phys. 40 (1969) 2837.
[7] C.E. Patton, J. Appl. Phys. 41 (1970) 431.
[8] W. Haubenreisser, D. Linzen, Phys. Stat. Sol. 2 (1962) 734.
[9] W. Haubenreisser, D. Linzen, Phys. Stat. Sol. 3 (1963) 133.
[10] G.A. Petrakovskii, Izv. Vyssh. Uchebn. Zaved. Fiz. 6 (1962) 29.
[11] Y.M. Yakovlev, Y.N. Burdin, Sov. Phys. Solid State 16 (1974) 301.
[12] C.E. Patton, Phys. Stat. Sol. B 92 (1979) 211.
[13] E. Schlömann, R.I. Joseph, I. Bady, J. Appl. Phys. 34 (1963) 672.
[14] J.J. Green, B.J. Healy, J. Appl. Phys. 34 (1963) 1285.
[15] S. Dixon, A. Tauber, R.O. Savage, J. Appl. Phys. 36 (1965) 1018.
[16] J. Helszajn, J. McStay, IEEE Trans. Microwave Theory Tech. MTT-18 (1970) 518.
[17] J. Helszajn, J. Mcstay, IEEE Tans. Microwave Theory Tech. MTT-20 (1972) 437.
[18] M.V. Kogekar, P. Kabos, C.E. Patton, J. Appl. Phys. 55 (1984) 2524.
[19] A.G. Gurevich, A.V. Nazarov, O.A. Chivileva, V.V. Petrov, Phys. Solid State 41 (1999) 1513.
[20] R.G. Cox, C.E. Patton, M.A. Wittenauer, P. Kabos, L. Chen, J. Appl. Phys. 89 (2001) 4454.
[21] A.V. Nazarov, R.G. Cox, C.E. Patton, IEEE Trans. Magn. 37 (2001) 2380.
[22] A.G. Gurevich, G.A. Melkov, Magnetic Oscillations and Waves, CRC Press, New York, 1996.
[23] M. Sparks, Ferromagnetic Relaxation Theory, McGraw Hill Publ. Co., New York, 1964.
[24] M.J. Hurben, C.E. Patton, J. Appl. Phys. 83 (1998) 4344.